Received: 8 September 2019 | Revised: 1 November 2019 | Accepted: 12 November 2019

DOI: 10.1002/ese3.565

RESEARCH ARTICLE

Energy Science & Engineering Open Access

Experimental investigation on dynamic strength and energy dissipation characteristics of gas outburst-prone coal

Chaojun Fan[1,2,3] | **Sheng Li**[1,2] | **Derek Elsworth**[3] | **Jun Han**[1] | **Zhenhua Yang**[1]

[1]College of Mining, Liaoning Technical University, Fuxin, Liaoning Province, China

[2]State Key Laboratory for GeoMechanics and Deep Underground Engineering, China University of Mining & Technology, Xuzhou, Jiangsu Province, China

[3]Energy and Mineral Engineering, Pennsylvania State University, University Park, Pennsylvania, USA

Correspondence
Chaojun Fan, College of Mining, Liaoning Technical University, Fuxin, Liaoning Province, China.
Email: chaojunfan@139.com

Funding information
Research Fund of State Key Laboratory Cultivation Base for Gas Geology and Gas Control (Henan Polytechnic University), Grant/Award Number: WS2018B05; Open Projects of State Key Laboratory for GeoMechanics and Deep Underground Engineering of China, Grant/Award Number: SKLGDUEK1510; National Natural Science Foundation of China, Grant/Award Number: 51674132 and 51874159

Abstract

We report laboratory experiments to investigate the dynamic failure characteristics of outburst-prone coal using a split Hopkinson pressure bar (SHPB). For comparison, two groups of experiments are completed on contrasting coals—the first outburst-prone and the second outburst-resistant. The dynamic mechanical properties, failure processes, and energy dissipation of both outburst-prone and outburst-resistant coals are comparatively analyzed according to the obtained dynamic compressive and tensile stress-strain curves. Results show that the dynamic stress-strain response of both outburst-prone and outburst-resistant coal specimens comprises stages of compression, linear elastic deformation, then microfracture evolution, followed by unstable fracture propagation culminating in rapid unloading. The mechanical properties of both outburst-prone and outburst-resistant coal specimens exhibit similar features: The uniaxial compressive strength and indirect tensile strength increase linearly with the applied strain rate, and the peak strain increases nonlinearly with the strain rate, whereas the elastic modulus does not exhibit any clear strain rate dependency. Differences in the dynamic failure characteristics between outburst-prone and outburst-resistant coals also exist. The hardening effect of strain rate on outburst-prone coal is more apparent than on outburst-resistant coal, which is reflected in the dynamic increase factor at the same strain rate. However, the dynamic strength of outburst-prone coals is still lower than that of outburst-resistant coals due to its low quasi-static strength. The dissipated energy of outburst-prone coal is smaller than that of outburst-resistant coal. Therefore, the outburst-prone coal, characterized by low strength, high deformability, and small energy dissipation when dynamically loaded to failure, is more favorably disposed to the triggering and propagation of gas outbursts.

KEYWORDS

dynamic increase factor, dynamic strength, energy dissipation, outburst-prone coal, split Hopkinson pressure bar

1 | INTRODUCTION

Coal is the basic energy and fuel source in China. Coal and gas outbursts during underground coal mining are characterized by the sudden ejection of large masses of coals or volumes of gases.[1-4] Such outbursts may result in significant damage to equipment (Figure 1A) and may also result in injury and fatalities.[5-8] Since the first-recorded outburst happened in the Isaac coal mine in Lule coal field in 1843, more than 40 000 outbursts have been reported worldwide.[9] The most disastrous mine outbursts resulted in 187 deaths in the Nowa Ruda Colliery (Poland) in 1941, 148 deaths in the Daping coal mine (China) in 2004, and 214 deaths in the Sunjiawan coal mine (China) in 2005.[2,10,11] Much exploratory research over the past 100 years has probed this catastrophic phenomenon to obtain an improved understanding of the causative mechanisms and better mitigate outbursts.[6,12-18] However, few of the proposed mechanisms can be successfully applied to explain, predict, and prevent outbursts. Due to the unique characteristics of these destructive, short duration, and high-intensity events, outbursts are both unpredictable in space and time.[5,6,19,20] It remains difficult to accurately measure in situ stress and gas pressure or to examine coal properties at different scales and for varied impact loads.[21] Current wisdom is that outbursts are a violent dynamic instability of the coal mass when the interaction of abnormal geostresses, high gas pressures, and the presence of "outburst-prone" coal reaches a critical condition.[22] The divergence of different theories lies in the myriad of different reasons that this critical condition is reached. These include the stress-concentrating influence of faults, folds, the presence of gas pockets, the impacts of thickness variation in the coal seam, among others.[23,24] Although these theories commonly link the propensity for outbursting to the presence and action of "outburst-prone coal" (Figure 1), the key features of its dynamic failure characteristics under impact loading remain poorly understood and constrained.[25-32]

Although the quasi-static physical properties of coal and rock have been studied widely, the dynamic failure characteristics of coal and rock are less fully constrained.[5] Dynamic properties of interest include the following: density, wave velocity, porosity, strength, scale effect, bedding effect, the influence of moisture, and energy dissipation.[15,33-45] Very high loading rate dynamic tests are usually conducted by using split Hopkinson pressure bar (SHPB) systems,[30,46] to determine dynamic properties of brittle materials including concretes, ceramics, rocks, and coals under wide range of impact loadings or strain rates of 10^1-10^4/s.[47-53] For determination of dynamic properties of different coals, the principal attributes are to recovery the dynamic magnitudes of Young's modulus and compressive/tensile strength based on the stress-strain curves at very high strain rates.[43,45] For instance, scholars have investigated the stress-strain curves and energy dissipation of coals under different bedding orientations, dry or saturated coals.[54-56] Fractal characteristics and electromagnetic radiation of crack propagation of coal were tested during an SHPB test.[57,58] So far, extensive suites of dynamic SHPB tests have been carried on rock and common coal materials, but only a few such dynamic tests have been completed on outburst-prone coals.[59] The diversity of dynamic characteristics between prone and resistant coals was not reported. Here, we supplement this dearth of observations by recovering a full suite of dynamic failure and energy dissipation characteristics to contrast the response of outburst-prone coals against a control sample of outburst-resistant coals.

In this study, experiments on both outburst-prone and outburst-resistant/neutral coals are conducted under quasi-static and impact loading using the MTS815 and SHPB systems, respectively. The mechanical properties of both outburst-prone and outburst-resistant coals, including uniaxial compressive strength, indirect tensile strength, elastic modulus, peak strain, and dynamic strength increase factor are compared with strain rate and between coal types. The energy dissipation ratio is proposed to quantitatively describe the energy dissipation of coal responding to the incident energy. These provide the scientific underpinnings for causal mechanisms for the triggering and progress of outbursts.

2 | EXPERIMENTAL SETUP AND OBSERVATIONS

In this section, we investigate the principles and processes of experimental observations on both outburst-prone and

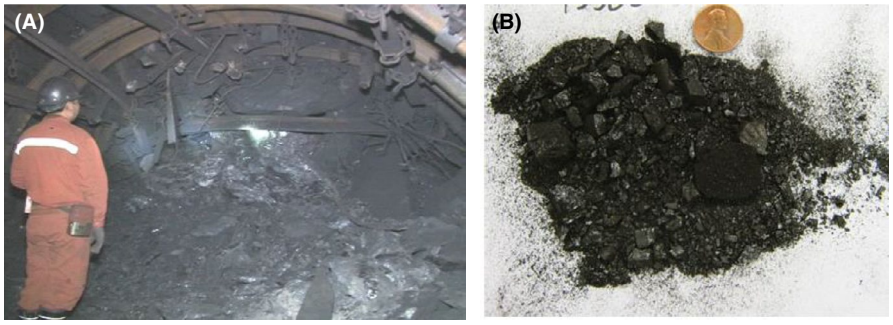

FIGURE 1 Fragmented coals: (a) outburst coal at advancing face in site; (b) laboratory dynamically failed coal

outburst-resistant/neutral coals in detail to identify their different quasi-static and dynamic failure characteristics. These include aspects of specimen preparation, composition of the SHPB system, theory and basic principles of SHPB tests, and experimental procedures.

2.1 | Specimen procurement and preparation

We collected large fresh coal block samples from the 4th coal seam of the Xintian coal mine in Guizhou Province, China. Due to the large-scale coal and gas outburst accident occurred in 4th coal seam of the Xintian coal mine on 5 October 2014, the coal is generally considered as outburst-prone coal. The coal is characterized by high in situ gas pressure ($p_g = 2.5$ MPa), small hardiness coefficient ($f = 0.5$), and low permeability ($k = 0.0218$ mD). The gas adsorption constant is 26.1 m^3/t, and the initial velocity of gas emission is 11.2 mmHg. As measured by proximate analysis, the Xintian coal is anthracite with a vitrinite reflectance of 2.13%, moisture content of 1.91%, ash content of 23.28%, volatile matter of 8.81%, and fixed carbon of 66%.

As a comparison, we also collected coal block samples from the 11th coal seam of the Xinzhouyao coal mine in Shanxi Province, China. There is no coal and gas outburst accident happened in Xinzhouyao coal mine during the mining history. This coal is generally an outburst-resistant coal and is characterized by low gas pressure ($p_g = 0.23$ MPa), large hardiness coefficient ($f = 4.4$), and high permeability ($k = 0.756$ mD). The gas adsorption constant and the initial velocity of Xinzhouyao coal were not measured. Meanwhile, the Xinzhouyao coal is bituminous coals with a vitrinite reflectance of 0.85%, moisture content of 5.83%, ash content of 14.35%, volatile matter of 2.32%, and fixed carbon of 57.5%. Compared with the Xinzhouyao coal, the Xintian coal is featured by greater vitrinite component and higher metamorphic degree.

The coal blocks were wrapped immediately after cutting and recovery to prevent oxidation and drying during transportation. According to the ISRM suggested methods, specimens with a slenderness ratio of $L_s/D_s = 1{:}1$ (50 mm × 50 mm) and a slenderness ratio of $L_s/D_s = 0.5{:}1$ (25 mm × 50 mm) were drilled from the block samples for dynamic uniaxial compressive strength tests and indirect tensile strength tests (Brazilian split), respectively.[60,61] The two ends of the cylindrical specimens were cut and ground to ensure flatness ±0.05 mm and parallelism ±0.02 mm, and for use in the SHPB tests. A subset of the prepared coal specimens are shown in Figure 2.

The quasi-static mechanical properties of the coal specimens were measured by an MTS815 hydraulic servo-controlled testing system with all measurements made at room temperature. The capacity of the load frame is 100 kN, and displacement control of 1.0 mm/min was used for the uniaxial compressive tests and 0.2 mm/min for the Brazilian split tensile tests. The results of these tests are shown in Figure 3. It can be calculated that the quasi-static compressive strength of Xintian (prone) and Xinzhouyao (resistant) coals are 4.76 and 11.45 MPa, respectively. The quasi-static tensile strength of Xintian and Xinzhouyao coals are 0.68 and 1.45 MPa, respectively. Above information illustrates that the quasi-static strength of Xintian coal is much weaker than that of Xinzhouyao coal.

2.2 | Experimental apparatus of SHPB and its basic principles

Dynamic compressive and tensile strength tests on the outburst-prone and outburst-resistant coals were conducted using the SHPB system at the State Key Laboratory for GeoMechanics and Deep Underground Engineering. A schematic diagram and photograph of the SHPB system are shown in Figure 4. The SHPB system consists of a launching device, pressure bars, an energy absorption device, and a signal acquisition and processing system. The launching device comprises a high pressure gas cylinder and gas gun. The pressure bar includes a striker bar, an incident bar, and a transmitting bar. The energy absorption device includes an absorbing bar and a deceleration unit. Finally, the signal acquisition and processing system includes strain gauges and a data acquisition device, and a data processing device to filter noise and analyze the results.

To more accurately obtain the dynamic properties of the coal specimens, a square rubber sheet is used as a pulse shaper. This transforms the incident stress wave from a rectangular wave to an approximately sinusoidal form. Vaseline is applied to both ends of the coal specimens to minimize transverse strain caused by the stress wave. As shown in Figure 5, significant lateral vibrations do not occur during the stress wave propagation. This implies that the SHPB system propagates an essentially

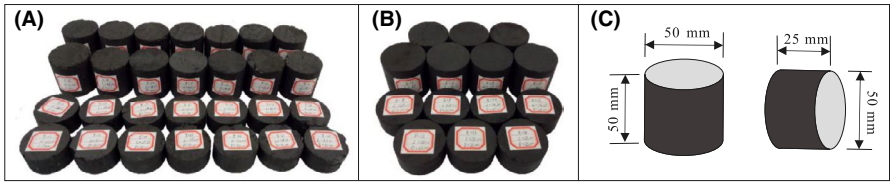

FIGURE 2 Experimental coal specimens, (a) Xintian coal specimen with outburst-prone, (b) Xinzhouyao coal specimen with outburst-resistant, and (c) size of coal specimens

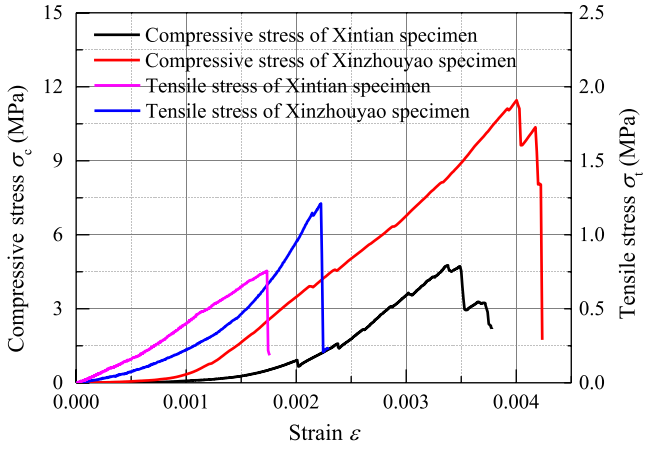

FIGURE 3 Quasi-static compressive and tensile stress-strain curves

one-dimensional wave. Additionally, the strain of the transmitted wave is basically equal to that of the sum of the incident and reflected waves. Thus, the SHPB apparatus also satisfies conditions of stress homogeneity. The rising edge of the incident wave reaches 90 s, which provides sufficient time for the coal specimen to achieve a homogeneous impact stress. Force equilibrium is achieved by preparing specimens with a small slenderness ratio and in maintaining good contact between pressure bars and coal specimens. Slenderness ratios of L_s/D_s = 1:1 and L_s/D_s = 0.5:1 were selected for compressive and tensile SHPB tests, respectively.

In the SHPB tests, coal specimens are placed between the incident bar and the transmitting bar. The striker bar is launched by a compressed gas gun and collides with the incident bar. The collision induces a longitudinal elastic compressive stress wave (incident compressive pulse, ε_i) in the incident bar. The stress wave then propagates through the incident bar and impacts the coal specimen causing a high rate of deformation.[51] The strain rate delivered to the coal specimen is controlled by varying the striking velocity. When the stress wave propagates to the interface between the coal specimen and the incident bar, it is reflected by and transmitted to the incident and transmitting bars. Parts of the incident pulse are reflected back into the incident bar as a reflected tensile pulse, ε_r, while others travel through the specimen into the transmission bar as a transmitted compressive pulse, ε_t. Strain gauges on the incident bar and transmitted bar measure the pulse signals and record them to the data acquisition device.

Wave theory is adopted to express the stress-strain curve of the coal material[37]:

$$\begin{cases} \gamma(t) = \dfrac{C_b}{L_s}\left(\varepsilon_i - \varepsilon_r - \varepsilon_t\right) \\ \varepsilon(t) = \dfrac{C_b}{L_s}\displaystyle\int_0^t \left(\varepsilon_i - \varepsilon_r - \varepsilon_t\right) dt \\ \sigma(t) = \dfrac{A_b}{2A_s} E_b \left(\varepsilon_i + \varepsilon_r + \varepsilon_t\right) \end{cases} \tag{1}$$

where γ is strain rate; E_b is elastic modulus of the pressure bar, GPa; C_b is the velocity of the stress wave in the pressure bar, m/s; A_b is the cross-sectional area of the pressure bar, m^2; A_s is the original cross-sectional area of the coal specimen, m^2; and L_s is the length of coal specimen, m.

The impact stresses on both ends of the coal specimen are calculated as[54]:

$$\begin{cases} P_1(t) = A_b E_b \left(\varepsilon_i + \varepsilon_r\right) \\ P_2(t) = A_b E_b \varepsilon_t \end{cases} \tag{2}$$

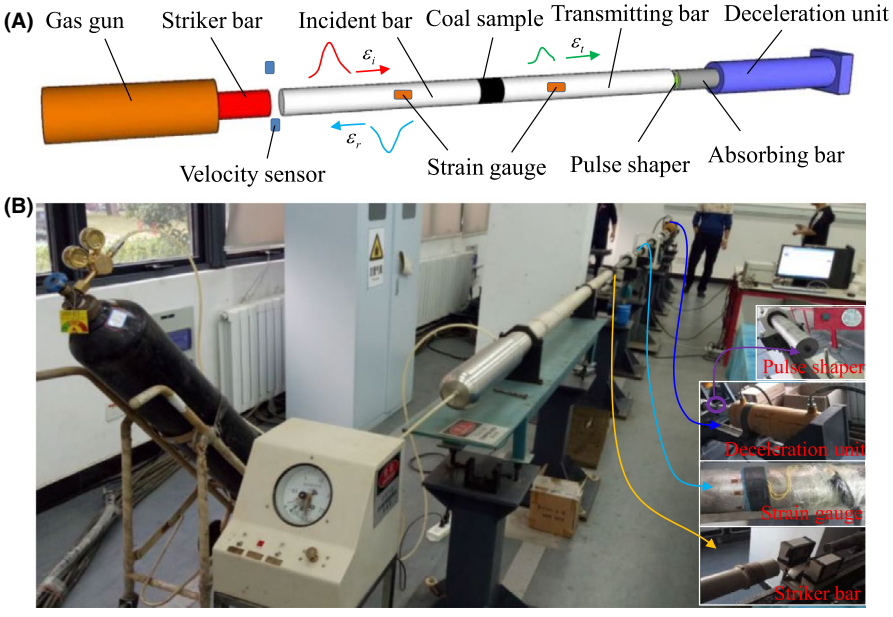

FIGURE 4 The split Hopkinson pressure bar apparatus, (a) schematic diagram and (b) photograph

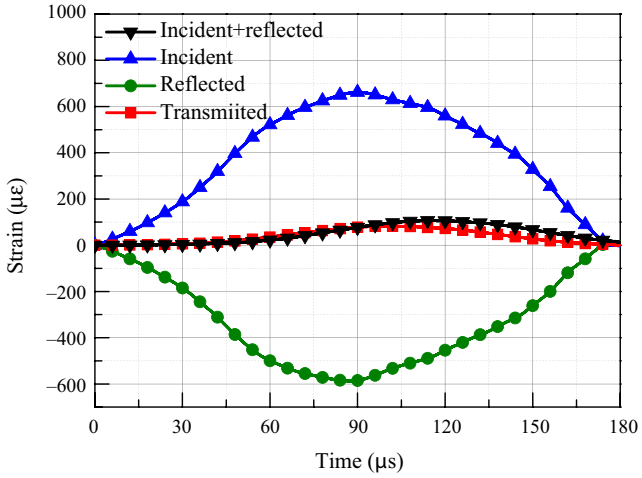

FIGURE 5 Strain balance checking for a typical split Hopkinson pressure bar test

Based on the stress homogeneity hypothesis, the impact stress balance on both ends of the coal specimen is achieved by satisfying $P_1(t) = P_2(t)$. The above equation can be rewritten as[62]:

$$\varepsilon_i + \varepsilon_r = \varepsilon_t \tag{3}$$

By submitting Equation (3) into Equation (1), the strain rate, dynamic strain, and dynamic stress are recovered as:

$$\begin{cases} \gamma(t) = -\dfrac{2c_b}{l_s}\varepsilon_r \\ \varepsilon(t) = -\dfrac{2c_b}{l_s}\displaystyle\int_0^t \varepsilon_r dt \\ \sigma(t) = \dfrac{A_b}{A_s}E_b\varepsilon_t \end{cases} \tag{4}$$

Finally, the stress-strain curves of coal specimens under impact loads can be obtained by calculating the measured signals of the reflected and transmitted pulses using Equation (4).

2.3 | Experimental procedure of SHPB test

To identify the contrasting dynamic failure characteristics separating outburst-prone from outburst-resistant coals, and to better understand the dynamic failure process, a number of uniaxial compressive SHPB tests and indirect tensile SHPB tests were completed.

For the compressive SHPB tests, a group of 14 coal specimens (Y1-Y14) from the Xintian (outburst-prone) coal mine were loaded to failure, with measured average strain rates varying from 17.18/s to 110.73/s; as a comparison, another group of 7 coal specimens (X1-X7) from the Xinzhouyao (outburst-resistant) coal mine were also conducted, with the measured average strain rates varying from 22.76/s to 105.54/s. A further group of 12 coal specimens (Y15-Y26) from the Xintian coal mine and 6 coal specimens (X8-X13) from the Xinzhouyao coal mine were selected to conduct tensile SHPB tests, with the measured average strain rates varying from 17.25/s to 89.89/s and from 15.62/s to 96.27/s, respectively.

The strain rate in the coal specimen is largely dependent on the striker bar velocity. The relationship between the average strain rate and striker bar velocity for the compressive and tensile SHPB tests is shown in Figure 6. At high speed, the incident bar delivers large kinetic energy. When the incident bar impacts the coal specimen, stress wave propagates and forces both rapid deformation and a high strain rate. The average strain rate of the coal specimen increases with an increase in the striker bar velocity. A least squares fit of the data yields the exponential relation for the SHPB tests.

3 | RESULTS AND DISCUSSION

We explore the impact of strain rate on the mechanical characteristics of coals—to define key features that control outburst potential, including dynamic deformation moduli, peaks strengths, and the ability to dissipate energy.

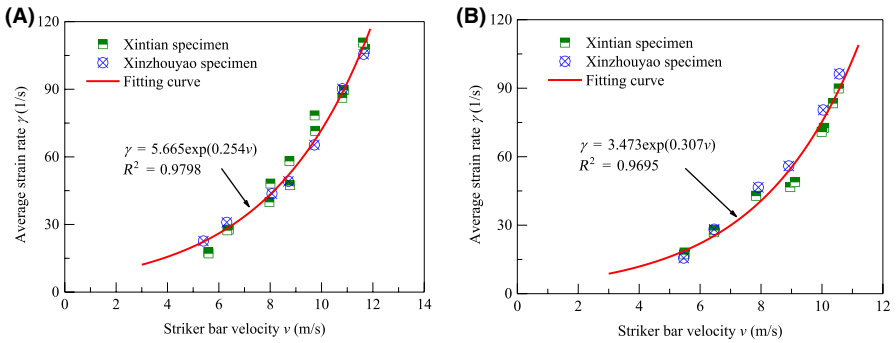

FIGURE 6 Relationship between average strain rate and striker bar velocity: (a) uniaxial compressive and (b) indirect tensile SHPB tests

3.1 | Effect of strain rate on mechanical properties

The dynamic compressive stress-strain curves of the Xinzhouyao (resistant) and Xintian (prone) coal specimens are shown in Figure 7A and 7B, respectively. The dynamic compressive stress paths of both outburst-prone and outburst-resistant coal specimens are significantly strain-rate–dependent. For instance, the peak compressive stress (uniaxial compressive strength) of the Xinzhouyao specimen increases from 12.59 to 47.8 MPa when the strain rate increases from 22.76/s to 105.54/s, while this value of the Xintian specimens increases from 5.23 to 26.12 MPa when the strain rate increases from 17.80/s to 107.91/s.

The dynamic tensile stress-strain curves of the Xinzhouyao (resistant) and Xintian (prone) coal specimens are shown in Figure 8A and 8, respectively. Affected by the adhesion of the strain gauge on the incident bar, the incident and reflected pulse signals of coal specimen Y23 were not detected and recorded—there is no dynamic tensile stress-strain curve for this coal specimen in Figure 8B. The strain-rate–dependent response is apparent from the dynamic tensile stress-strain curves. The tensile strength increases with an increase in strain rate. For instance, the peak tensile stress (indirect tensile strength) of the Xinzhouyao specimen increases from 1.67 to 6.91 MPa when the strain rate varies from 15.62/s to 96.27/s, while this value of the Xintian specimen increases from 0.95 to 3.62 MPa when the strain rate varies from 18.04/s to 89.89/s. Compared with Xinzhouyao coal, the Xintian coal has a smaller uniaxial compressive strength and indirect tensile strength, which implies that the outburst-prone coal is usually weaker in both compression and tension than the outburst-resistant coal.

Based on the dynamic stress-strain curves in Figures 7 and 8, we propose an ensemble characteristic response curve to characterize the key features of the stress-strain behavior. The typical dynamic stress-strain curve of coal comprises five stages: compression, linear elastic deformation, microcrack initiation, unstable crack growth, and unloading,[35,39] as shown in Figure 9.

The first stage on stress-strain curve is compression (stage 1). In this stage, the incident and transmitting bars are not completely contacted with the coal sample. The residual space and microfractures within coal sample will be compacted gradually. Accompanying by the closure of microfractures, the deformation resistance of the coal sample increases macroscopically. The second stage is the linear elastic deformation (stage 2), showing a linear increase trend. External loads are not sufficient to accelerate fracture growth or to generate new fractures within the coal sample. This can only result in stable reversible deformations. In this stage, the elastic state of the coal sample remains unchanged, and the elastic energy is accumulating. The slope of the stress-strain curve keeps constant, which represents the Young's modulus. The stage followed by linear elastic

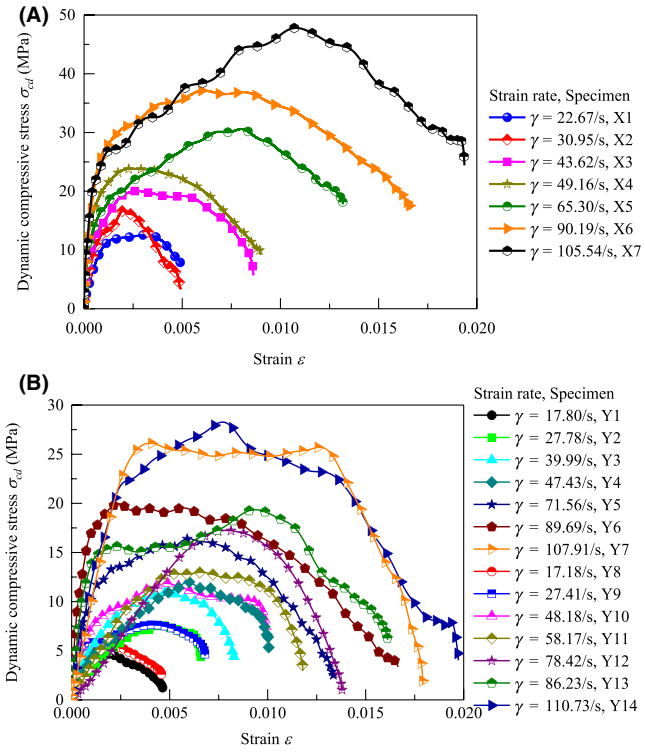

FIGURE 7 Dynamic stress-strain curves of coal specimens in compressive SHPB test: (a) Xinzhouyao (outburst-resistant) and (b) Xintian (outburst-prone) coal specimens

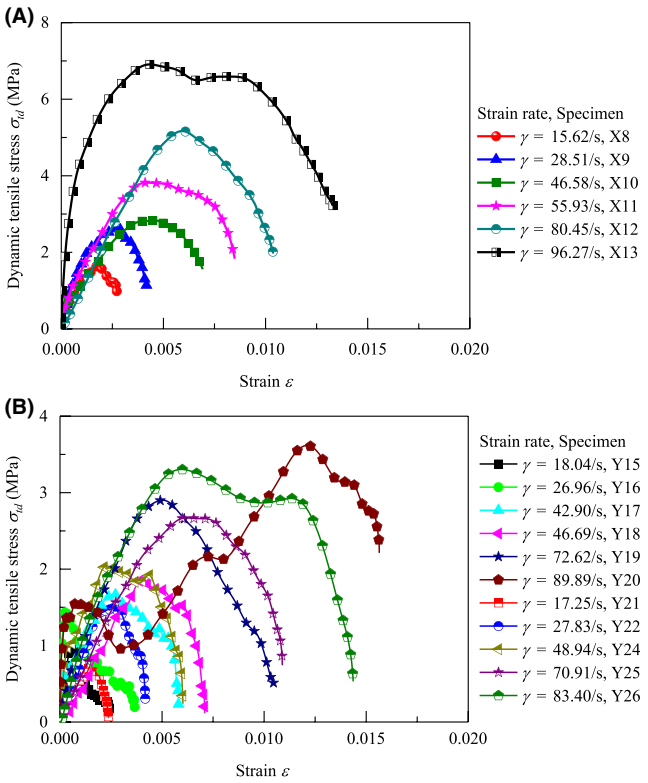

FIGURE 8 Dynamic stress-strain curves of tensile SHPB tests: (a) Xinzhouyao (resistant) and (b) Xintian (prone) coal specimens

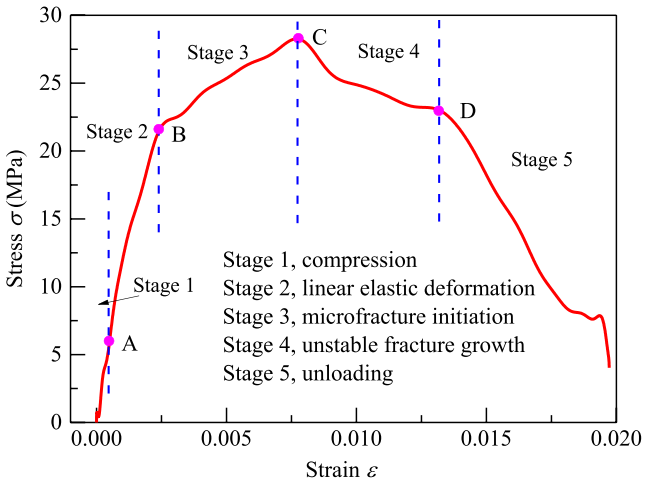

FIGURE 9 Typical dynamic stress-strain curve of coal specimen

deformation is the microfracture initiation (stage 3). The increasing trend of stress slows down with the coal strain, showing an upward convex. In this stage, the microfractures within the coal sample expand and produce new fractures. Plastic deformation gradually dominates as a deformation mode. After that, the coal sample enters the unstable fracture growth stage (stage 4). The fractures expand quickly, and many newly generated fractures connect with the primary fractures caused by the accumulated energy release. On point D, the peak stress achieves and the slope of the curve approaches zero. This point corresponds to the peak strain. The final stage is characterized by the rapid unloading (stage 5). The stress-strain curve decreases rapidly, indicating the completely rapture of coal sample. The bearing capacity of the sample decreases at full speed. The contact surface between the pressure bar and the coal sample becomes uneven, resulting in a variety of curve shapes during unloading, as manifested by various curves in Figures 7 and 8.

In Figure 7, the peak compressive stress increases with strain rate in both cases. Some characteristic parameters, such as the stress-strain gradient in the linear elastic stage and the peak strain in the unstable crack propagation stage, are diverse for each curve. As strain rate increases, the microfracture evolution and unstable fracture propagation stage (stages 3 and 4) are prolonged in both temporal duration and strain ranges, leading to these two stages becoming more significant at higher strain rates. In other words, with the advantage of spatial extension and temporal duration, the cracks within specimens initiate and propagate more rapidly, inducing more dissipation of accumulated energy during these two stages. Then, the stress-strain curves corresponding to different strain rates enter the rapid unloading stage. When comparing the response of outburst-prone and outburst-resistant coals, the outburst-prone coal is more ductile with wide postpeak region and a more significant phase of rapid unloading. The higher strain rate of the coal specimen will lead to a wider range of plastic strain, as well as greater energy dissipation. The stress-strain curves with high strain rates usually decline slightly after reaching the peak value, then enter a plastic plateau, before finally dropping at the conclusion of the test.

In Figure 8, similar features are observed—the peak tensile stress and peak strain increase with the strain rate. Under the same strain rate, the tensile strength of outburst-prone coal is smaller than that of outburst-resistant coal. Normally, the curve rapidly unloads after reaching a peak tensile stress—indicating that the outburst-resistant coal is more brittle.

We extract key features of the dynamic stress-strain curves (Figures 7 and 8), including peak compressive stress, peak tensile stress, strain at peak stress, elastic modulus, and dissipated energy during the entire process of dynamic loading, and compile and present them in Tables 1 and 2.

The key mechanical properties including peak compressive stress, peak tensile stress, peak strain, and elastic modulus are plotted in Figure 10. The peak compressive stress and the peak tensile stress increase linearly with strain rate; the strain at peak compressive stress increases nonlinearly, while the scattered points representing the evolution of elastic modulus are disordered, indicating that the elastic modulus has no obvious relationship with strain rate.

The dynamic increase factor (DIF) is defined as the ratio of dynamic strength to static strength, which reflects the increase in mechanical strength of coal under impact (strain rates). This parameter includes two indexes, the dynamic increase factor for the compressive strength (DIF_c) and the dynamic increase factor for the tensile strength (DIF_t). These are expressed as:

$$\begin{cases} \mathrm{DIF}_c = \dfrac{\sigma_{c,d}}{\sigma_{c,s}} \\ \mathrm{DIF}_t = \dfrac{\sigma_{t,d}}{\sigma_{t,s}} \end{cases} \tag{5}$$

where $\sigma_{c,d}$ and $\sigma_{c,s}$ are the dynamic and static uniaxial compressive strengths, respectively; $\sigma_{t,d}$ and $\sigma_{t,s}$ are the dynamic and static indirect tensile strengths, respectively.

Figure 11 displays the variation of the dynamic increase factors (DIF_c and DIF_t) with different strain rates. The dynamic increase factors increase linearly with strain rate. The rate dependences of DIF_c at strain rates of 17.18/s-110.73/s for Xintian (prone) and of 22.67/s-105.54/s for Xinzhouyao (resistant) coals are fitted as:

$$\begin{cases} \mathrm{DIF}_c = 0.0467(\gamma) + 0.2611 \\ \mathrm{DIF}_c = 0.0351(\gamma) + 0.3097 \end{cases} \tag{6}$$

The rate dependences of DIF_t at a strain rate of 17.25/s-89.89/s for Xintian (prone) coal and at 15.62/s-96.27/s for Xinzhouyao (resistant) coals are fitted as:

$$\begin{cases} \mathrm{DIF}_t = 0.0523(\gamma) + 0.4305 \\ \mathrm{DIF}_t = 0.0421(\gamma) + 0.3755 \end{cases} \tag{7}$$

TABLE 1 Dynamic uniaxial compressive properties of coal specimens

Coal source	Specimen number	Specimen length (mm)	Striker bar velocity (m/s)	Average strain rate (1/s)	Uniaxial compressive strength (MPa)	Elastic modulus (GPa)	Strain at peak stress
Xinzhouyao coal mine (resistant)	X1	50.00	5.40	22.67	12.59	14.54	0.00314
	X2	50.15	6.31	30.95	16.67	21.18	0.00199
	X3	50.20	8.07	43.62	20.09	28.35	0.00272
	X4	50.00	8.71	49.16	23.82	72.54	0.00246
	X5	49.85	9.72	65.30	30.59	22.66	0.00799
	X6	50.10	10.81	90.19	37.15	44.33	0.00612
	X7	50.05	11.64	105.54	47.80	27.18	0.01079
Xintian coal mine (prone)	Y1	50.12	5.59	17.80	5.23	14.92	0.00111
	Y2	50.10	6.39	27.78	7.60	2.70	0.00449
	Y3	49.60	7.97	39.99	10.93	5.06	0.00479
	Y4	49.52	8.77	47.43	12.03	3.13	0.00592
	Y5	49.60	9.75	71.56	16.40	13.68	0.00596
	Y6	49.70	10.87	89.69	19.96	30.64	0.00338
	Y7	50.10	11.70	107.91	26.12	9.79	0.01266
	Y8	51.05	5.60	17.18	5.84	26.37	0.00146
	Y9	50.13	6.33	27.41	7.66	21.19	0.00417
	Y10	50.00	8.01	48.18	11.87	10.36	0.00479
	Y11	51.30	8.75	58.17	12.99	3.41	0.00662
	Y12	50.00	9.73	78.42	17.25	2.66	0.00791
	Y13	50.25	10.81	86.23	19.35	19.79	0.00936
	Y14	49.30	11.61	110.73	28.27	11.15	0.00771

TABLE 2 Dynamic indirect tensile properties of coal specimens

Coal source	Specimen number	Specimen length (mm)	Striker bar velocity (m/s)	Average strain rate (1/s)	Indirect tensile strength (MPa)	Strain at peak stress
Xinzhouyao coal mine (resistant)	X8	24.70	5.46	15.62	1.67	0.00181
	X9	25.25	6.46	28.21	2.65	0.00273
	X10	24.65	7.91	46.58	2.83	0.00455
	X11	25.25	8.91	55.93	3.82	0.00417
	X12	24.81	10.04	80.45	5.17	0.00588
	X13	25.20	10.57	96.27	6.91	0.00431
Xintian coal mine (prone)	Y15	24.13	5.49	18.04	0.95	0.000541
	Y16	24.65	6.45	26.96	1.45	0.000287
	Y17	25.25	7.84	42.90	1.67	0.00262
	Y18	25.10	8.96	46.69	1.78	0.00281
	Y19	25.10	10.06	72.62	2.90	0.00497
	Y20	25.00	10.55	89.89	3.62	0.01211
	Y21	25.00	5.48	17.25	0.77	0.00157
	Y22	25.00	6.47	27.83	1.49	0.00262
	Y23	25.20	7.87	—	—	—
	Y24	25.42	9.12	48.94	2.04	0.00209
	Y25	25.25	9.99	70.91	2.67	0.00615
	Y26	25.30	10.36	83.41	3.30	0.00592

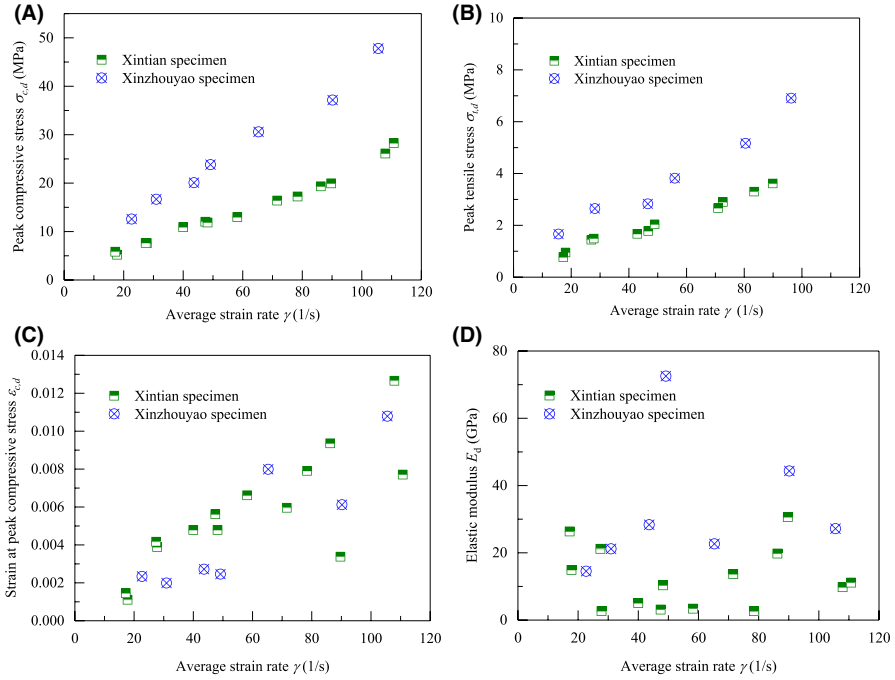

FIGURE 10 Dynamic mechanical properties of outburst-prone and outburst-resistant coal specimens: (a) peak compressive stress, (b) peak tensile stress, (c) strain at peak compressive stress, (d) elastic modulus

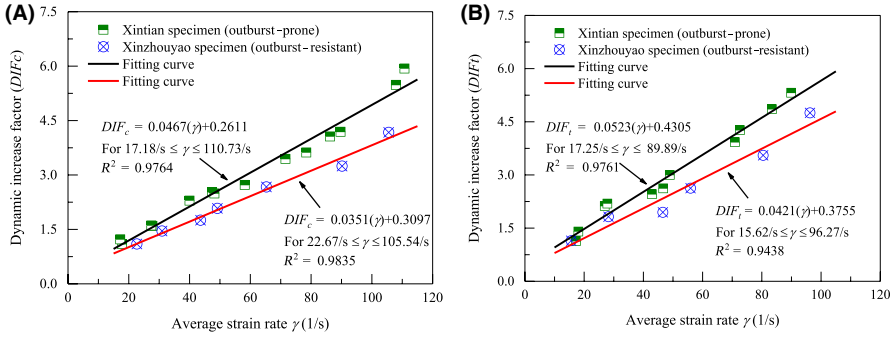

FIGURE 11 Relationship between the dynamic increase factor and strain rate for (a) uniaxial compressive strength and (b) indirect tensile strength

The dynamic increase factors (DIF_c and DIF_t) of outburst-prone coal are greater than those of outburst-resistant coal on the whole, indicating that the strain rate hardening effect of outburst-prone coal is more apparent than outburst-resistant coal. With the increase in impact loading, both dynamic compressive strength and tensile strength of outburst-prone coal rise faster than those of outburst-resistant coal. However, the dynamic strength of outburst-prone coal is still smaller than that of the outburst-resistant coal.

3.2 | Effect of strain rate on energy dissipation characteristics

The dynamic effect on energy dissipation is fundamentally reflected by the combined action of stress and strain of the coal specimen. During the entire process of dynamic loading and unloading, the energy carried by incident, reflected, and transmitted waves is expressed as [57,63]:

$$\begin{cases} E_i = \dfrac{A_b C_b}{E_b} \int \sigma_i^2 dt = A_b E_b C_b \int \varepsilon_i^2 dt \\ E_r = \dfrac{A_b C_b}{E_b} \int \sigma_r^2 dt = A_b E_b C_b \int \varepsilon_r^2 dt \\ E_t = \dfrac{A_b C_b}{E_b} \int \sigma_t^2 dt = A_b E_b C_b \int \varepsilon_t^2 dt \end{cases} \tag{8}$$

where E_i, E_r, and E_t are the incident energy, reflected energy, and transmitted energy, respectively, kJ; σ_i, σ_r, and σ_t are the stresses corresponding to the incident, reflected, and transmitted waves in the pressure bar, respectively, MPa.

The dissipated energy of the coal specimen is given by[63]:

$$E_d = E_i - E_r - E_t \tag{9}$$

The energy dissipation coefficient (C_d), defined as the ratio of dissipated energy to incident energy, is given by:

$$C_d = E_d / E_i \tag{10}$$

Figure 12 shows the energy dissipation characteristics of both outburst-prone and outburst-resistant coals in the uniaxial compressive SHPB tests. The dissipated energy increases exponentially with the impact time. Initially, the coal specimen is elastic, and the amount of dissipated energy is small. As impact time increases, the specimen gradually becomes plastic (stages 3, 4, and 5) with the continuous generation of cracks, and their accumulation and expansion—the dissipated energy sharply increases. The faster the impact speed, the larger the strain rate, and the shorter the time taken for the destruction of the coal. Comparing Figure 12A, the energy dissipation of the Xintian (prone) and Xinzhouyao (resistant) specimens appears similar—the dissipated energy increases with an increase in the strain rate. Nevertheless, the dissipated energy of Xinzhouyao specimen (resistant) is larger than that of the Xintian specimen (prone). As shown in Figure 12B, the dissipated energy of the Xintian specimen ranges from 1.106 to 12.279 kJ when the strain rate varies from 17.18/s to 110.73/s, while the dissipated energy of the Xinzhouyao specimen ranges from 3.323 to 23.076 kJ when the strain rate varies from 22.67/s to 105.54/s. The dissipated energy of both Xinzhouyao and Xintian specimens exponentially increases with the strain rate, which are respectively expressed as:

Figure 12C shows the variation of incident energy, reflected energy, transmitted energy, and dissipated energy during the

$$\begin{cases} E_{\mathrm{d}} = 2.29\exp(0.0221\gamma) \\ E_{\mathrm{d}} = 1.084\exp(0.0218\gamma) \end{cases} \tag{11}$$

entire dynamic failure process of the coal specimens. For the same coal specimen at a specific strain rate, the incident energy > reflected energy > dissipated energy > transmitted energy. Meanwhile, these values of the Xinzhouyao specimen (resistant) are greater than those of Xintian specimen (prone). As shown in Figure 12D, the energy dissipation coefficient of the Xintian specimen (prone) is much smaller than that of Xinzhouyao specimen (resistant) under compressive impact loads. The energy dissipation coefficient increases linearly with strain rate, and their relationships are expressed as:

$$\begin{cases} C_{\mathrm{d}} = 0.0561\gamma + 29.077 \\ C_{\mathrm{d}} = 0.1118\gamma + 15.191 \end{cases} \tag{12}$$

Figure 13 shows the energy dissipation characteristics of the indirect tensile SHPB tests. Also, the dissipation energy increases exponentially with the impact time. The larger strain rate will lead to a shorter duration of coal dynamic failure. The dissipated energy of the Xinzhouyao specimen (resistant) is larger than that of the Xintian specimen (prone). The dissipated energy of the Xintian specimen ranges from 0.061 to 0.373 kJ when the strain rate varies from 17.25/s to 89.89/s, and the dissipated energy of the Xinzhouyao specimen ranges from 0.128 to 1.299 kJ when the strain rate varies from 15.62/s to 96.27/s. The dissipated energy of both Xinzhouyao and Xintian specimens increases exponentially with strain rate, which can be respectively expressed as:

For a specific strain rate, the incident energy, reflected energy, dissipated energy, and transmitted energy of the

$$\begin{cases} E_{\mathrm{d}} = 0.0545\exp(0.0216\gamma) \\ E_{\mathrm{d}} = 0.0879\exp(0.0278\gamma) \end{cases} \tag{13}$$

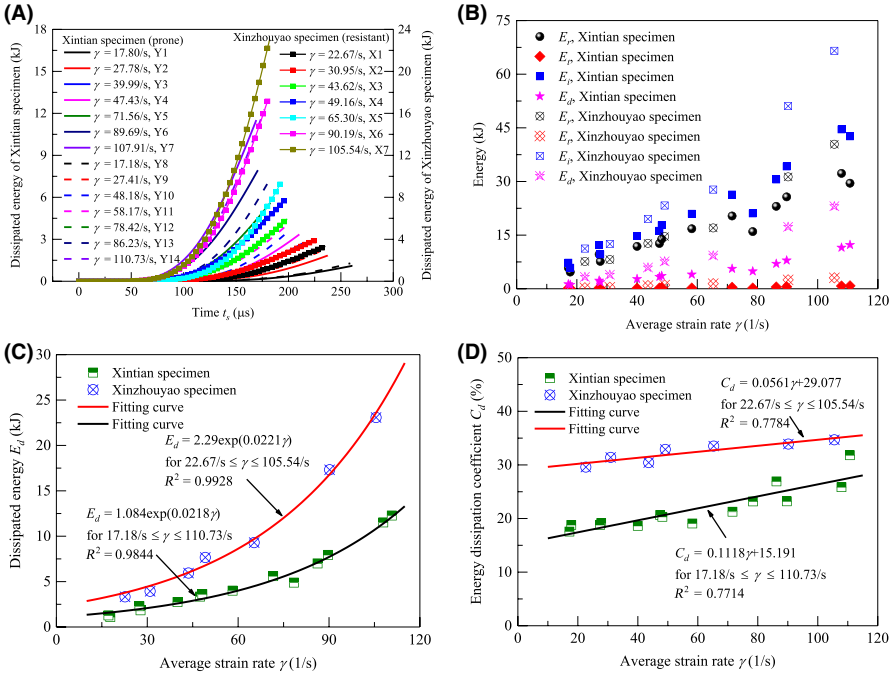

FIGURE 12 Dynamic energy characteristics of uniaxial compressive SHPB tests at different strain rates: (a) dissipated energy of Xintian (prone) and Xinzhouyao (resistant) specimens, (b) energy transition, and (c) effect of strain rate on dissipated energy, and (d) energy dissipation coefficient

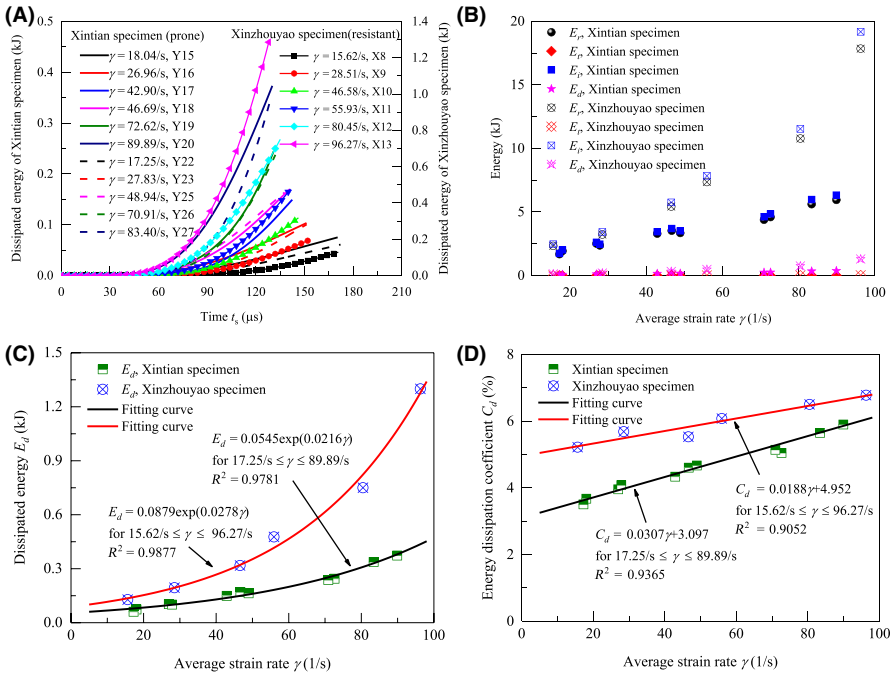

FIGURE 13 Dynamic energy characteristics of indirect tensile SHPB tests at different strain rates: (a) dissipated energy evolution of Xintian (prone) and Xinzhouyao (resistant) specimen, (b) energy transition, (c) effect of strain rate on dissipated energy, (d) energy dissipation coefficient

Xinzhouyao specimen (resistant) over the entire dynamic failure process are greater than those of the Xintian specimen (prone). The energy dissipation coefficient of the Xintian specimen is also smaller than that of the Xinzhouyao specimen under tensile impact loads. The energy dissipation coefficient of both Xintian and Xinzhouyao specimens increases linearly with strain rate:

$$\begin{cases} C_{\mathrm{d}} = 0.0188\gamma + 4.952 \\ C_{\mathrm{d}} = 0.0307\gamma + 3.097 \end{cases} \tag{14}$$

It is apparent from the above that the dissipated energy of outburst-prone coal during the dynamic failure process is less than that of outburst-resistant coal under the same degree of impact loading. This may be the reason why the compressive strength and tensile strengths of outburst-prone coal are smaller, and why outburst-prone coal is easier to rupture.

3.3 | Discussion on the dynamic failure characteristics of gas outburst-prone coal

Coal and gas outburst is a kind of dynamic disaster occurred during underground mining. Large masses of coals or volumes of gases are suddenly ejected or expelled into working space in few seconds. It takes only a certain milliseconds or microseconds for the outburst coal to be damaged from initial compression. The dynamic characteristics of energy dissipation and mechanical properties of coal may provide the scientific underpinnings for causal mechanisms of outbursts. Many scholars have investigated the dynamic properties by carrying extensive suites of dynamic SHPB tests on rock and common coal materials. However, fewer tests have been completed to identify the dynamic properties on both outburst-prone and outburst-resistant coals.[59] The distinguishment of dynamic characteristics between prone and resistant coals has not been reported. In this study, we conducted experiments on outburst-prone coals against a control sample of outburst-resistant coals under impact loading. The dynamic properties of dynamically failed coal, including uniaxial compressive strength, indirect tensile strength, elastic modulus, peak strain, and dynamic increase factor, together with energy dissipation, were recovered and compared between coal types. Both similar and distinct features of outburst-prone and outburst-resistant coals were obtained.

The mechanical properties exhibited similar change trends: The compressive and tensile strengths increased linearly with the applied strain rate, and the peak strain nonlinearly increased with the strain rate. Meanwhile, most of the dynamic stress-strain curves comprised stages of compression, linear elastic deformation, microfracture evolution, then followed by unstable fracture propagation culminating in rapid unloading. The shape of these curves was commonly occurred in many rocks. For instance, Li et al[51] and Feng et al[35] examined the dynamic mechanical properties of coal measures sandstone after thermal treatment and coal, respectively, and the stage divisions of stress-strain curves were put forward. The five stages in our works proposed a specific definition and elaboration for each stage.

Under the similar impact loading, the tensile or compressive strength of outburst-prone coals is lower than that of outburst-resistant coals. The dynamic increase factor of outburst-prone coals is greater than that of outburst-resistant coals, indicating

that the hardening effect of strain rate on outburst-prone coal is more apparent than on outburst-resistant coal. This phenomenon usually occurs in the impact tests on both coals and rocks. Chakraborty[37] investigated three Himalayan rocks (dolomite, quartzite, and limestone) under the same impact loading and found the dynamic increase factor of soft rocks was greater than that of hard rocks. Zhang[59] obtained a similar predicate after series of SHPB tests on coals. Although outburst-prone coal had greater dynamic increase factor than resistant coal, its dynamic strength is still lower than that of outburst-resistant coals due to its much lower quasi-static strength. Meanwhile, the dissipated energy of outburst-prone coal is smaller than that of outburst-resistant coal.

Overall, the outburst-prone coals are commonly characterized by low mechanical strength and high deformability, and small energy dissipation when loaded dynamically to failure. The dynamic failure of outburst-prone coal likely promotes rapid gas desorption into fractures from the coal matrix, and may accelerate the free gas carrying potential for the pulverized coal to enter the mining space and to trigger and participate in outbursts. The fragment distribution and microstructure evolution of dynamically crushed coal were not studied in this paper. These works will be done in the future researches.

4 | CONCLUSIONS

In this paper, both dynamic uniaxial compressive and indirect tensile tests are conducted on outburst-prone and outburst-resistant coals using a split Hopkinson pressure bar (SHPB) system. A full suite of dynamic failure characteristics are comparatively analyzed to contrast the response of outburst-prone coals against a control sample of outburst-resistant coals. These characterizations include the dynamic strength, failure processes, and energy dissipation. The following conclusions can be drawn:

1. The dynamic stress-strain response of both outburst-prone and outburst-resistant coal specimens primarily comprises five stages. In the first compression stage, the residual space and microfractures are compacted gradually. In the linear elastic deformation stage, the external loads are not sufficient to accelerate fracture growth, resulting in stable reversible deformations. Followed by the microfracture initiation stage, the microfractures expand to produce new fractures, and the plastic deformation dominates. In the final stage, the fractures expand quickly and connected with each other. When the peak stress achieves, the coal becomes completely raptured.
2. The compressive strength and tensile strength increase linearly with the applied strain rate, while the elastic modulus shows no clear trend with strain rate. Due to a greater dynamic increase factor (DIF), the strain rate hardening effect of outburst-prone coal is more obvious than that of outburst-resistant coal. However, the dynamic strength of outburst-prone coal is still smaller because of its lower quasi-static strength.
3. The dynamic energy dissipation of both outburst-prone and outburst-resistant coals exhibits similar trends. The higher the applied strain rate, the shorter the time required for full destruction of the coal. The dissipated energy increases exponentially with strain rate, while the energy dissipation coefficient increases only linearly. Under identical impact loading, the dissipated energy of outburst-resistant coal is larger than that of outburst-prone coal.

ACKNOWLEDGMENT

The author(s) would like to thank all editors and anonymous reviewers for their comments and suggestions. This research was financially supported by the National Natural Science Foundation of China (Grant Nos. 51674132 and 51874159), the Open Projects of State Key Laboratory for GeoMechanics and Deep Underground Engineering of China (No. SKLGDUEK1510), and the Research Fund of State Key Laboratory Cultivation Base for Gas Geology and Gas Control (Henan Polytechnic University) (Grant No. WS2018B05).

CONFLICT OF INTEREST

The authors declare no competing financial interest.

ORCID

Chaojun Fan https://orcid.org/0000-0003-4578-0760

REFERENCES

1. Beamish BB, Crosdale PJ. Instantaneous outbursts in underground coal mines: an overview and association with coal type. *Int J Coal Geol*. 1998;35(1–4):27-55.
2. Lama RD, Bodziony J. Management of outburst in underground coal mines. *Int J Coal Geol*. 1998;35(1–4):83-115.
3. Fan C, Elsworth D, Li S, Zhou L, Yang Z, Song Y. Thermo-hydro-mechanical-chemical couplings controlling CH_4 production and CO_2 sequestration in enhanced coalbed methane recovery. *Energy*. 2019;173:1054-1077.
4. Wang C, Yang S, Li X, Li J, Jiang C. Comparison of the initial gas desorption and gas-release energy characteristics from tectonically-deformed and primary-undeformed coal. *Fuel*. 2019;238:66-74.
5. Fan C, Elsworth D, Li S, et al. Modelling and optimization of enhanced coalbed methane recovery using CO_2/N_2 mixtures. *Fuel*. 2019;253:1114-1129.
6. Wang S, Elsworth D, Liu J. Rapid decompression and desorption induced energetic failure in coal. *J Rock Mech and Geotech Eng*. 2015;7(3):345-350.
7. Hu QT, Zhou SN, Zhou XQ. Mechanical mechanism of coal and gas outburst process. *J China Coal Soc*. 2008;33(12):1368-1372.

8. Liu T, Lin B, Yang W, et al. Dynamic diffusion-based multifield coupling model for gas drainage. *J Nat Gas Sci Eng*. 2017;44:233-249.
9. Fan C, Li S, Luo M, Du W, Yang Z. Coal and gas outburst dynamic system. *Int J Min Sci Technol*. 2017;27(1):49-55.
10. Zhang ZM, Zhang YG. Investigation into coal-gas outburst occurred in Daping Coal mine, by using theories of gas-geology. *J China Coal Soc*. 2005;30(2):137-140.
11. Huo B, Jing X, Fan C, Han Y. Numerical investigation of flue gas injection enhanced underground coal seam gas drainage. *Energ Sci Eng*. 2019. https://doi.org/10.1002/ese3.491
12. Wang C, Yang S, Yang D, Li X, Jiang C. Experimental analysis of the intensity and evolution of coal and gas outbursts. *Fuel*. 2018;226:252-262.
13. Liu T, Lin B, Yang W, Zou Q, Kong J, Yan F. Cracking process and stress field evolution in specimen containing combined flaw under uniaxial compression. *Rock Mech Rock Eng*. 2016;49(8):3095-3113.
14. Qin L, Zhai C, Xu J, Liu S, Zhong C, Yu G. Evolution of the pore structure in coal subjected to freeze−thaw using liquid nitrogen to enhance coalbed methane extraction. *J Petrol Sci Eng*. 2019;175:129-139.
15. Zhao W, Cheng Y, Guo P, Jin K, Tu Q, Wang H. An analysis of the gas-solid plug flow formation: new insights into the coal failure process during coal and gas outbursts. *Powder Technol*. 2017;305:39-47.
16. Fan C, Li S, Luo M, Yang Z, Lan T. Numerical simulation of hydraulic fracturing in coal seam for enhancing underground gas drainage. *Energ Explor Exploit*. 2019;37(1):166-193.
17. Liu H, Lin B, Mou J, Yang W. Mechanical evolution mechanism of coal and gas outburst. *Rock Mech Rock Eng*. 2018;52:1591-1597.
18. Wang C, Yang S, Li J, Li X, Jiang C. Influence of coal moisture on initial gas desorption and gas-release energy characteristics. *Fuel*. 2018;232:351-361.
19. Zhao W, Cheng Y, Jiang H, Jin K, Wang H, Wang L. Role of the rapid gas desorption of coal powders in the development stage of outbursts. *J Nat Gas Sci Eng*. 2016;28:491-501.
20. Xue Y, Gao F, Liu X. Effect of damage evolution of coal on permeability variation and analysis of gas outburst hazard with coal mining. *Nat Hazards*. 2015;79(2):999-1013.
21. Song H, Jiang Y, Elsworth D, Zhao Y, Wang J, Liu B. Scale effects and strength anisotropy in coal. *Int J Coal Geol*. 2018;195:37-46.
22. Yin G, Jiang C, Wang JG, Xu J, Zhang D, Huang G. Huang GA new experimental apparatus for coal and gas outburst simulation. *Rock Mech Rock Eng*. 2016;49(5):2005-2013.
23. Han J, Zhang HW. The controlling of tectonic evolution to coal and gas outburst. *J China Coal Soc*. 2010;35(7):1125-1130.
24. Qu Z, Wang GG, Jiang B, Rudolph V, Dou X, Li M. Experimental study on the porous structure and compressibility of tectonized coals. *Energ Fuel*. 2010;24(5):2964-2973.
25. Liu M, He X. Electromagnetic response of outburst-prone coal. *Int J Coal Geol*. 2001;45(2–3):155-162.
26. Jiang C, Xu L, Li X, et al. Identification model and indicator of outburst-prone coal seams. *Rock Mech Rock Eng*. 2015;48(1):409-415.
27. Wang G, Li W, Wang P, Yang X, Zhang S. Deformation and gas flow characteristics of coal-like materials under triaxial stress conditions. *Int J Rock Mech Min Sci*. 2017;91:72-80.
28. Song Y, Jiang B, Shao P, Wu JH. Matrix compression and multifractal characterization for tectonically deformed coals by Hg porosimetry. *Fuel*. 2018;211:661-675.
29. Song Y, Jiang B, Liu JG. Nanopore structural characteristics and their impact on methane adsorption and diffusion in low to medium tectonically deformed coals: case study in the Huaibei coal field. *Energ Fuel*. 2017;31(7):6711-6723.
30. Zhang QB, Zhao J. A review of dynamic experimental techniques and mechanical behaviour of rock materials. *Rock Mech Rock Eng*. 2014;47(4):1411-1478.
31. Xia K, Huang S, Jha AK. Dynamic tensile test of coal, shale and sandstone using split Hopkinson pressure bar: a tool for blast and impact assessment. *Int J Geotech Earthquake Eng*. 2010;1(2):24-37.
32. Feng J, Wang E, Chen X, Ding H. Energy dissipation rate: an indicator of coal deformation and failure under static and dynamic compressive loads. *Int J Min Sci Technol*. 2018;28(3):397-406.
33. Mambou LN, Ndop J, Ndjaka JMB. Theoretical investigations of mechanical properties of sandstone rock specimen at high temperatures. *Min Sci Technol*. 2014;50(1):69-80.
34. Ju Y, Sudak L, Xie H. Study on stress wave propagation in fractured rocks with fractal joint surfaces. *Int J Solids Struct*. 2007;44(13):4256-4271.
35. Feng J, Wang E, Chen L, Li X, Xu Z, Li G. Experimental study of the stress effect on attenuation of normally incident P-wave through coal. *J Appl Geophys*. 2016;132:25-32.
36. Qi L, Tang X, Wang Z, Peng X. Pore characterization of different types of coal from coal and gas outburst disaster sites using low temperature nitrogen adsorption approach. *Int J Min Sci Technol*. 2017;27(2):371-377.
37. Chakraborty T, Mishra S, Loukus J, Halonen B, Bekkala B. Characterization of three Himalayan rocks using a split Hopkinson pressure bar. *Int J Rock Mech Min Sci*. 2016;85:112-118.
38. Fakhimi A, Azhdari P, Kimberley J. Physical and numerical evaluation of rock strength in Split Hopkinson Pressure Bar testing. *Comput Geotech*. 2018;102:1-11.
39. Li M. Research on rupture mechanisms of coal measures sandstone under high temperature and impact load. Ph.D dissertation: China University of Mining and Technology, Xuzhou, China, 2014.
40. Zhao Y, Gong S, Hao X, Peng Y, Jiang Y. Effects of loading rate and bedding on the dynamic fracture toughness of coal: laboratory experiments. *Eng Fract Mech*. 2017;178:375-391.
41. Liu X, Dai F, Zhang R, Liu J. Static and dynamic uniaxial compression tests on coal rock considering the bedding directivity. *Environ Earth Sci*. 2015;73(10):5933-5949.
42. Wang M, Zhu Z, Dong Y, Zhou L. Study of mixed-mode I/II fractures using single cleavage semicircle compression specimens under impacting loads. *Eng Fract Mech*. 2017;177:33-44.
43. Zhao YX, Xiao H, Huang YQ. Dynamic split tensile test of Brazilian disc of coal with split Hopkinson pressure bar loading. *J China Coal Soc*. 2014;39(2):286-291.
44. Li M, Mao X, Lu A, et al. Effect of specimen size on energy dissipation characteristics of red sandstone under high strain rate. *Int J Min Sci Technol*. 2014;24(2):151-156.
45. Wang W, Wang H, Li D, Li H, Liu Z. Strength and failure characteristics of natural and water-saturated coal specimens under static and dynamic loads. *Shock Vib*. 2018;2018:1-15.
46. Xia K, Yao NW. Dynamic rock tests using split Hopkinson (Kolsky) bar system–a review. *J Rock Mech and Geotech Eng*. 2015;7(1):27-59.
47. Luo X, Xu JY, Bai EL, Li W. Research on the dynamic compressive test of highly fluidized geopolymer concrete. *Con Build Mat*. 2013;48:166-172.

48. Ravichandran G, Subhash G. Critical appraisal of limiting strain rates for compression testing of ceramics in a split Hopkinson pressure bar. *J Am Ceram Soc*. 1994;77(1):263-267.
49. Frew DJ, Forrestal MJ, Chen W. Pulse shaping techniques for testing brittle materials with a split Hopkinson pressure bar. *Exp mech*. 2002;42(1):93-106.
50. Zhu WC, Bai Y, Li XB, Niu LL. Numerical simulation on rock failure under combined static and dynamic loading during SHPB tests. *Int J Impact Eng*. 2012;49:142-157.
51. Li M, Mao X, Cao L, Pu H, Mao R, Lu A. Effects of thermal treatment on the dynamic mechanical properties of coal measures sandstone. *Rock Mech Rock Eng*. 2016;49(9):3525-3539.
52. Gong F, Ye H, Luo Y. The effect of high loading rate on the behaviour and mechanical properties of coal-rock combined body. *Shock Vib*. 2018.
53. Li CW, Wei SY, Wang XY, Liu JK, Lei DJ. Experiment of dynamic property and transient magnetic effects of coal during deformation and fracture. *J Coal Sci Eng*. 2012;18(3):258-261.
54. Zhao Y, Liu S, Jiang Y, Wang K, Huang Y. Dynamic tensile strength of coal under dry and saturated conditions. *Rock Mech Rock Eng*. 2016;49(5):1709-1720.
55. Zhao Y, Zhao GF, Jiang Y, Elsworth D, Huang Y. Effects of bedding on the dynamic indirect tensile strength of coal: laboratory experiments and numerical simulation. *Int J Coal Geol*. 2014;132:81-93.
56. Zhao YX, Gong S, Huang YQ. Experimental study on energy dissipation characteristics of coal samples under impact loading. *J China Coal Soc*. 2015;40(10):2320-2326.
57. Zhao Y, Gong S, Zhang C, Zhang Z, Jiang Y. Fractal characteristics of crack propagation in coal under impact loading. *Fractals*. 2018;26(2):1840014.
58. Li CW, Wang QF, Lyu PY. Study on electromagnetic radiation and mechanical characteristics of coal during an SHPB test. *J Geophys Eng*. 2016;13(3):391.
59. Zhang WQ.Study on mechanical property of soft coal under impact load and its effect to coal and gas outburst. Dissertation: AnHui University of Science and Technology, Huainan, China, 2014.
60. ISRM. Commission on standardization of laboratory and field tests. Suggested methods for determining tensile strength of rock materials. *Int J Rock Mech Min Sci Geomech Abstr*. 1978;15:99-103.
61. Yang Z, Fan C, Lan T, et al. Dynamic mechanical and microstructural properties of outburst-prone coal based on compressive SHPB tests. *Energies*. 2019;12(22):4236.
62. Cao LL, Pu H, Li M, Mao XB, Zhang LY. Experimental research on the dynamic tensile fracture and the energy dissipation characteristics of coal-serial sandstone. *J China Coal Soc*. 2017;42(2):492-499.
63. Li JC, Rong LF, Li HB, Hong SN. An SHPB test study on stress wave energy attenuation in jointed rock masses. *Rock Mech Rock Eng*. 2018;52:403-420.

How to cite this article: Fan C, Li S, Elsworth D, Han J, Yang Z. Experimental investigation on dynamic strength and energy dissipation characteristics of gas outburst-prone coal. *Energy Sci Eng*. 2019;00:1–14. https://doi.org/10.1002/ese3.565